NUMERICAL INVESTIGATION OF DIFFUSION COMBUSTION IN TURBULENT REACTING GAS FLOWS

Ismatulla Khujaev,
Dilshodjon Ergashev
Institute of Mechanics and Seismic Stability of Structures named after M.T.Urazbaev, Uzbekistan Academy of Sciences, Tashkent, Uzbekistan
Corresponding author ErgashevD.Y.
E-mail: dilshod77m@gmail.com

Abstract: *This study presents a numerical approach for modeling axisymmetric methane diffusion combustion in an unbounded co-flowing oxidizer stream. The formulation is based on the governing equations of a turbulent boundary layer, transformed using Mises variables to facilitate the analysis. To simplify the multi-component conservation equations, the Schwab–Zeldovich function is introduced, reducing the system to a single scalar equation.*

A two-layer, four-point nonlinear difference scheme with second-order accuracy in the streamwise direction is employed to solve the resulting equations. Due to the inherent nonlinearity of the governing system, an iterative method is implemented. Selected outcomes of the numerical simulation are discussed to illustrate the behavior of key physical parameters under turbulent combustion conditions.

Keywords: *Turbulent jet, diffusion flame, gas mixture, velocity field, total enthalpy, Schwab–Zeldovich function, finite difference method, numerical simulation.*

1. Introduction

Natural gas remains the dominant source of thermal energy globally, accounting for approximately 70% of the energy produced and consumed. The remaining 30% is derived from alternative sources such as hydropower, wind, solar, and nuclear energy. Despite its prevalence, the thermal efficiency of both natural and liquefied gas combustion systems remains relatively low.

This inefficiency has prompted a growing interest in understanding and optimizing combustion processes—specifically, flame initiation and propagation mechanisms. Recent advancements in turbulence modeling, injection dynamics, and combustion theory have led to the refinement of mathematical models that describe these phenomena.

Among the various approaches developed for continuous combustion, two primary methods are widely used in turbulent boundary layer regimes. In the first

approach, the fuel and oxidizer are introduced separately into the combustion region, leading to the development of a diffusion flame. In contrast, the second method involves premixing the fuel with the oxidizer—typically air or an oxygen-enriched mixture—prior to injection.

Each method offers distinct advantages in controlling flame characteristics such as length, width, temperature distribution, and particulate formation. These factors are essential in the design and optimization of combustion chambers and burners, necessitating robust theoretical analysis.

Theoretical studies in this field continue to evolve, as the fundamental understanding of exothermic chemical reactions under turbulent flow conditions remains incomplete. Given the complex nature of such flows and the significance of combustion in energy production, continued research is essential. In practical applications, combustion can be organized either in batch systems or in high-pressure continuous reactors, where reactants are steadily introduced and combustion products are removed in a controlled manner [1]. In the second approach to combustion organization, reactive components may be introduced either as separate streams or as a pre-mixed formulation [7]. These combustion strategies are typically analyzed within the frameworks of either diffusion-based or premixed (uniform) combustion models [8].

Premixed combustion models are exemplified by classical configurations such as the Bunsen burner and are governed by Arrhenius-type reaction kinetics or chemical equilibrium models [9]. In contrast, diffusion combustion models—most notably those introduced by Burke and Schumann and further developed by Schwab and Zeldovich—assume that chemical reactions occur at an infinitely fast rate across an infinitesimally thin flame front [10]. This idealization simplifies the mathematical treatment of combustion zones and has proven effective in modeling high-temperature processes involving gaseous fuels.

Notably, this theoretical model was adapted for specific gaseous fuels by F. Aliyev and Z. Zhumayev. Despite the assumption of instantaneous reaction rates, diffusion flames often exhibit significant spatial extent due to transport limitations, making this model particularly relevant in industrial contexts such as rotary kilns, construction material processing, and mercury production. These applications benefit from the model’s capacity to predict temperature fields and optimize conditions for simultaneous heat and mass transfer.

However, a survey of the literature [3, 7–10] reveals that methane-based diffusion combustion—despite methane being the dominant component of natural gas—has not been sufficiently investigated. In Uzbekistan, methane accounts for the majority of extracted natural gas, largely due to the depletion of gas reservoirs and the

selective removal of heavier hydrocarbons via single- or multi-stage cryogenic separation processes. Given these circumstances, the present study focuses on methane dispersion and its diffusion flame characteristics under turbulent flow conditions.

The physical model considers a methane jet issuing from a circular nozzle into a co-flowing oxidizing environment. The interacting gas streams possess distinct thermophysical properties and compositions. The combustion process occurs with such high reaction rates that oxidizer penetration into the fuel zone is negligible, and vice versa. In this setting, chemically inert species undergo convective transport and molecular diffusion, interacting with reactive components primarily through physical mechanisms rather than chemical transformation.

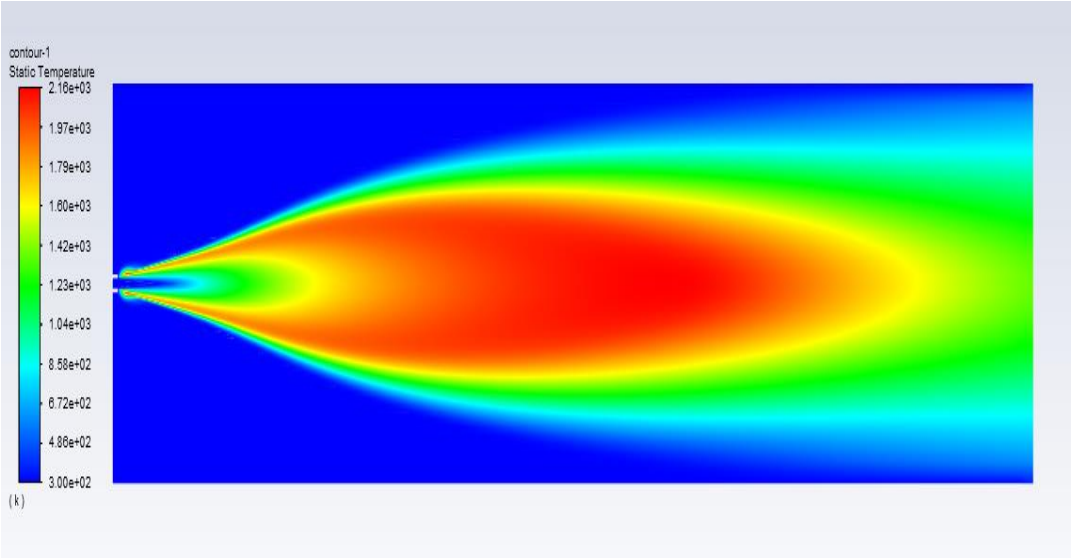

Figure 1. Submerged jet with diffusion torch showing the thermal structure—color-mapped temperature, labeled isotherms, and locations of peak *T* along the jet centerline.

The combustion process is represented by a stoichiometric equation describing an irreversible overall reaction.

Mathematical problem definition. Thermal interaction and mass transfer processes

$$\begin{cases} \rho u\dfrac{\partial u}{\partial x}+\rho\vartheta\dfrac{\partial u}{\partial r}=\dfrac{1}{r}\dfrac{\partial}{\partial r}\left(\rho(\nu+\nu_t)r\dfrac{\partial u}{\partial r}\right), \\ \dfrac{\partial(\rho u r)}{\partial x}+\dfrac{\partial(\rho\vartheta r)}{\partial r}=0, \\ \rho u\dfrac{\partial H}{\partial x}+\rho\vartheta\dfrac{\partial H}{\partial r}=\dfrac{1}{\mathrm{Pr}\,r}\dfrac{\partial}{\partial r}\left(\rho(\nu+\nu_t)r\dfrac{\partial H}{\partial r}\right), \\ \rho u\dfrac{\partial c_2}{\partial x}+\rho\vartheta\dfrac{\partial c_2}{\partial r}=\dfrac{1}{Sc\,r}\dfrac{\partial}{\partial r}\left[\rho\left(\dfrac{1}{\mathrm{Re}}+\nu_t\right)r\dfrac{\partial c_2}{\partial r}\right]+\omega_2, \\ \rho u\dfrac{\partial c_n}{\partial x}+\rho\vartheta\dfrac{\partial c_n}{\partial r}=\dfrac{1}{Sc\,r}\dfrac{\partial}{\partial r}\left[\rho\left(\dfrac{1}{\mathrm{Re}}+\nu_t\right)r\dfrac{\partial c_n}{\partial r}\right]+\omega_n \quad (n=1,3,4...N). \end{cases} \tag{1}$$

The system of differential equations is accompanied by algebraic relations describing the enthalpy and the state of the gas mixture.

$$H = c_p T + c_2 h_2^*,\ c_p = \sum_{k=1}^{N} c_{pn} c_n,$$
$$p = \rho \frac{R_0}{m} T = const,\quad m = \left(\sum_{n=1}^{N} m_n / c_n \right)^{-1}, \qquad (2)$$

Equation system [3,5,9]. Here u, v- Longitudinal and radial velocity distributions m/s; ρ, T- Density of the gas $\left(\kappa g\, m^{-3}\right)$ together with absolute temperature (K); Pr, Sc - Turbulent Prandtl and Schmidt numbers c_k - Concentration of components by mass; ω_k - Mass combustion rate $\left(kg\, m^{-3}\, s^{-1}\right)$; ν_t – turbulent viscosity; H - full enthalpy;

The conditions governing entry into the flow region are as follows

$$x = 0: \begin{cases} u = u_2, H = H_2, \tilde{C} = 1,\ k = k_2,\ \varepsilon = \varepsilon_2, v = 0 \quad 0 \le y \le a \\ u = u_1, H = H_1, \tilde{C} = 0,\ k = k_1,\ \varepsilon = \varepsilon_1,\ v = 0 \quad a < y \le \infty \end{cases}$$
$$x > 0: \begin{cases} \frac{du}{dy} = v = \frac{dH}{dy} = \frac{d\tilde{C}}{dy} = \frac{dk}{dy} = \frac{d\varepsilon}{dy} = 0, \quad y = 0 \\ u \to u_1,\ v \to 0,\ H \to H_1,\ \tilde{C} \to 0, k \to k_1,\ \varepsilon \to \varepsilon_1 \quad y \to y_\infty \end{cases} \qquad (3)$$

Modeling turbulence. The $k - \varepsilon$ model was employed in the representation of turbulent exchange [1-3]:

$$\begin{cases} \rho u \frac{\partial k}{\partial x} + \rho \vartheta \frac{\partial k}{\partial r} = \frac{1}{\delta_\varepsilon r} \frac{\partial}{\partial r} \left(\rho r \nu_t \frac{\partial k}{\partial r} \right) + G_k - \rho \varepsilon, \\ \rho u \frac{\partial \varepsilon}{\partial x} + \rho \vartheta \frac{\partial \varepsilon}{\partial r} = \frac{1}{\delta_\varepsilon r} \frac{\partial}{\partial r} \left(\rho r \nu_t \frac{\partial \varepsilon}{\partial r} \right) + c_{\varepsilon 1} f_1 \frac{\varepsilon}{k} G_k - c_{\varepsilon 2} \rho f_2 \frac{\varepsilon^2}{k}. \end{cases} \quad \nu_t = \frac{c_\mu f_\mu k^2}{\varepsilon},\ R_R = \frac{\sqrt{k}\, r}{\nu},$$

$$f_1 = 1 + \left(\frac{A_1}{f_\mu} \right)^3,\ f_2 = 1 - e^{-R_t^2}, \qquad (4)$$

$$R_t = \frac{k^2}{\nu \varepsilon},\ f_\mu = \left(1 - e^{-A_\mu R_R}\right)^2 \left(1 + \frac{A_1}{R_t}\right),\quad G_k = 4 \rho \nu_t \left(\frac{\partial u}{\partial r} \right)^2,\ c_{\varepsilon 2} = 1.92,\ c_\mu = 0.09,\ \delta_k = 1,\ c_{\varepsilon 1} = 1.44,$$

$$\delta_\varepsilon = 1.3,\ A_1 = 0.05,\ A_\mu = 0.0165$$

To analyze the transport and combustion of methane in a co-flowing air stream, we consider a system where methane is uniformly distributed within the fuel jet. The chemical interaction between methane and the oxidizer is modeled using a global one-step irreversible reaction. The reaction can be expressed in stoichiometric form as:

$$v_2 A + v_1 O_2 \to v_3 CO_2 + v_4 H_2 O + h_2^*,$$

where stoichiometric coefficients $\nu_1 = 2.0$ $\nu_2 = 1$, $\nu_3 = 1.0$, $\nu_4 = 2.0$, Refer to oxygen, combustible, carbon monoxide and water vapor; $h_2^* = 55644$. In addition, the presence of molecular nitrogen is taken into account N_2, Which is considered a chemically passive component. Accordingly, in this case, the number of component retention equations is $N = 5$, which are abbreviated as $L(c_k) = \omega_k$ $(k = 1..5)$. Where $L(c_k) = \rho u \frac{\partial c_k}{\partial x} + \rho v \frac{\partial c_k}{\partial y} - \frac{1}{Sc\, y} \frac{\partial}{\partial y}\left(\rho \varepsilon y \frac{\partial c_k}{\partial y} \right)$ – Linear and uniform with respect to its argument - mass concentration k - component c_k operator, and ω_k – Mass rate of formation (disappearance) k - the diversity of molecules at a certain point of the flame front per time unit. For the reaction rate, the governing relations are introduced as follows:

$$\begin{aligned} &\omega_3 \nu_k m_k + \omega_k \nu_3 m_3 = 0 \quad \text{at} \quad k = 1, 2; \\ &\omega_3 \nu_k m_k - \omega_k \nu_3 m_3 = 0 \quad \text{at} \quad k = 4; \\ &\omega_1,\ \omega_2 \le 0,\ \omega_3,\ \omega_4 \ge 0. \end{aligned} \tag{5}$$

The relations provided indicate the method for excluding reaction rates from the governing component balance equations $L(c_k) = \omega_k$.

If the Schwab–Zeldovich functions are defined as

$$\tilde{C}_k = \begin{cases} c_3 \nu_k m_k + c_k \nu_3 m_3 = 0 & \text{при} \quad k = 1, 2; \\ c_3 \nu_k m_k - c_k \nu_3 m_3 = 0 & \text{при} \quad k = 4, \end{cases} \tag{6}$$

the conservation equations for components $k = 1, 2$ and 4 are reduced to the stock-free form $L(\tilde{C}_k) = 0$

The equation for inert gas concentration, since $\omega_5 = 0$, is also similar to $L(c_5) = 0$. I.e. Since the system provides four differential equations for five concentrations, the deficiency is compensated by applying the diffusion combustion model assumptions. The boundary conditions corresponding to the introduced functions can be written as follows:

$$\begin{aligned} &\left(\tilde{C}_1\right)_1 = (c_3)_1 \nu_1 m_1 + (c_1)_1 \nu_3 m_3, \quad \left(\tilde{C}_1\right)_2 = (c_3)_2 \nu_1 m_1, \\ &\left(\tilde{C}_2\right)_1 = (c_3)_1 \nu_2 m_2, \quad \left(\tilde{C}_2\right)_2 = (c_3)_2 \nu_2 m_2 + (c_2)_2 \nu_3 m_3, \\ &\left(\tilde{C}_4\right)_1 = (c_3)_1 \nu_4 m_4 - (c_4)_1 \nu_3 m_3, \quad \left(\tilde{C}_4\right)_2 = (c_3)_2 \nu_4 m_4 - (c_4)_2 \nu_3 m_3. \end{aligned} \tag{7}$$

At this stage, functions that are relatively redundant with respect to $\tilde{C}_k$ are introduced

$$\tilde{\tilde{C}}_k = \frac{\tilde{C}_k - \left(\tilde{C}_k\right)_1}{\left(\tilde{C}_k\right)_2 - \left(\tilde{C}_k\right)_1} = \frac{c_5 - (c_5)_1}{(c_5)_2 - (c_5)_1}. \tag{8}$$

Analysis shows that equations $L(\tilde{\tilde{C}}_k)=0$ are mutually equivalent because they have the same coefficients and boundary conditions. This will allow four equations $L(\tilde{\tilde{C}}_k)=0$ to go to a single equation $L\left(\tilde{\tilde{C}}\right)=0$.

The Schwab–Zeldovich function is designed such that it equals 1 at the inlet of the fuel region, representing pure fuel, and 0 at the oxidizer inlet and along the jet boundary, where only oxidizer is present. Owing to the axisymmetric configuration of the problem, the function maintains symmetry along the central jet axis.

Once the distribution of this function is known, the mass fraction of the inert component (e.g., nitrogen) can be readily computed using a simple algebraic relation derived from species balance. $C_5=(C_5)_1+\left[(C_5)_2-(C_5)_1\right]\tilde{\tilde{C}}$. $\tilde{C}_k=\left(\tilde{C}_k\right)_1+\left[\left(\tilde{C}_k\right)_2-\left(\tilde{C}_k\right)_1\right]\tilde{\tilde{C}}$

.

Substitution of values $\tilde{C}_k$, $\left(\tilde{C}_k\right)_2$, $\left(\tilde{C}_k\right)_1$ such constraints reduce to a system of linear equations.

$$\begin{cases} c_3\nu_1 m_1+c_1\nu_3 m_3=(c_3)_1\nu_1 m_1+(c_1)_1\nu_3 m_3+ \\ \quad +\left[(c_3)_2\nu_1 m_1-(c_3)_1\nu_1 m_1-(c_1)_1\nu_3 m_3\right]\tilde{\tilde{C}}, \\ c_3\nu_2 m_2+c_2\nu_3 m_3=(c_3)_1\nu_2 m_2+ \\ \quad +\left[(c_3)_2\nu_2 m_2+(c_2)_2\nu_3 m_3-(c_3)_1\nu_2 m_2\right]\tilde{\tilde{C}}, \\ c_3\nu_4 m_4-c_4\nu_3 m_3=(c_3)_1\nu_4 m_4-(c_4)_1\nu_3 m_3+ \\ \quad +\left[(c_3)_2\nu_4 m_4-(c_4)_2\nu_3 m_3-(c_3)_1\nu_4 m_4+(c_4)_1\nu_3 m_3\right]\tilde{\tilde{C}}. \end{cases} \quad (9)$$

Let's simplify a system:

$$\begin{cases} c_3+c_1\dfrac{\nu_3 m_3}{\nu_1 m_1}=(c_3)_1+(c_1)_1\dfrac{\nu_3 m_3}{\nu_1 m_1}+\left[(c_3)_2-(c_3)_1-(c_1)_1\dfrac{\nu_3 m_3}{\nu_1 m_1}\right]\tilde{\tilde{C}}, \\ c_3+c_2\dfrac{\nu_3 m_3}{\nu_2 m_2}=(c_3)_1+\left[(c_3)_2-(c_3)_1+(c_2)_2\dfrac{\nu_3 m_3}{\nu_2 m_2}\right]\tilde{\tilde{C}}, \\ c_3-c_4\dfrac{\nu_3 m_3}{\nu_4 m_4}=(c_3)_1-(c_4)_1\dfrac{\nu_3 m_3}{\nu_4 m_4}+ \\ +\left[(c_3)_2-(c_3)_1-\left((c_4)_2-(c_4)_1\right)\dfrac{\nu_3 m_3}{\nu_4 m_4}\right]\tilde{\tilde{C}}. \end{cases} \quad (10)$$

Since the reactant concentrations vanish at the flame front, the value of the relatively redundant function can be derived from the first two equations of the system:

$\tilde{\tilde{C}}^* = \left[1 + \frac{(c_2)_2}{(c_1)_1}\frac{\nu_1 m_1}{\nu_2 m_2}\right]^{-1}$ at $\tilde{\tilde{C}}^* < \tilde{\tilde{C}} \le 1$, Within the fuel region, no oxidant is present – $c_1 = 0$.

The solution of the system is

$$c_2 = \left[(c_2)_2 + (c_1)_1\frac{\nu_2 m_2}{\nu_1 m_1}\right]\tilde{\tilde{C}} - (c_1)_1\frac{\nu_2 m_2}{\nu_1 m_1},\ c_3 = (c_3)_1 + (c_1)_1\frac{\nu_3 m_3}{\nu_1 m_1} + \left[(c_3)_2 - (c_3)_1 - (c_1)_1\frac{\nu_3 m_3}{\nu_1 m_1}\right]\tilde{\tilde{C}},$$

$$c_4 = (c_4)_1 + (c_1)_1\frac{\nu_4 m_4}{\nu_1 m_1} + \left[(c_4)_2 - (c_4)_1 - (c_1)_1\frac{\nu_4 m_4}{\nu_1 m_1}\right]\tilde{\tilde{C}}. \quad (11)$$

Conditions $0 \le \tilde{\tilde{C}} < \tilde{\tilde{C}}^*$ oxidant zone where there is no fuel is determined $c_2 = 0$. For the remaining components, the concentrations are obtained from the formulae:

$$c_1 = (c_1)_1 - \left[(c_1)_1 + (c_2)_2\frac{\nu_1 m_1}{\nu_2 m_2}\right]\tilde{\tilde{C}},$$

$$c_3 = (c_3)_1 + \left[(c_3)_2 - (c_3)_1 + (c_2)_2\frac{\nu_3 m_3}{\nu_2 m_2}\right]\tilde{\tilde{C}}, \quad (12)$$

$$c_4 = (c_4)_1 + \left[(c_4)_2 - (c_4)_1 + (c_2)_2\frac{\nu_4 m_4}{\nu_2 m_2}\right]\tilde{\tilde{C}}.$$

The derived relations for concentrations may be checked through the summation of the component concentrations. Upon accounting for the dependencies

$$(c_2)_2 + (c_3)_2 + (c_4)_2 + (c_5)_2 = 1,$$

$$(c_1)_1 + (c_3)_1 + (c_4)_1 + (c_5)_1 = 1 \quad (13)$$

together with the mass balance derived from the stoichiometric reaction equation

$$\nu_1 m_1 + \nu_2 m_2 = \nu_3 m_3 + \nu_4 m_4 \quad (14)$$

The summation of concentrations within every zone is equal to one, while the mass concentrations of the components depend on the variable. $\tilde{\tilde{C}}$.

Therefore, once the value of the relative-redundant function $\tilde{\tilde{C}}$ is specified, both the flame front position and the component concentrations are determined unambiguously. The boundary conditions for this function are as outlined above:

$$\tilde{\tilde{C}}(0, y) = \begin{cases} 1 & 0 \le y \le a, \\ 0 & y > a, \end{cases} \quad \frac{\partial \tilde{\tilde{C}}(x,0)}{\partial x} = 0\ ,\ \tilde{\tilde{C}}(x, y_\infty) \to 0. \quad (15)$$

Chemical reaction with final rate modeling. The process of combustion is expressed in the form of a stoichiometric relation for the irreversible overall reaction: $CH_4 + 2O_2 = CO_2 + 2H_2O + h_2^*$, is here h_2^* – the thermal energy released in an exothermic reaction, while the reaction rate is represented by the Arrhenius law. [3]. $\omega_2 = A_{r1} c_1 c_2 \rho^2 \exp\left(-\frac{A_{r2}}{T}\right)$. Here entered designations

$$A_{r1} = -5,028 \cdot 10^{11} \frac{a\rho_2}{m_1 u_2},\ A_{r2} = \frac{200010.0}{8,31441}\,(K)$$

The presence of tangential velocity fluctuations at the interface between interacting gas streams, along with the existence of a high-temperature flame front within the heat and mass transfer region, signifies the turbulent nature of the flow in this domain. Given the dominant flow direction, the governing equations of a turbulent boundary layer are applicable for modeling the gas motion.

Introduction of nondimensional parameters together with Mises variables.

For the solution, characteristic values were employed to transform the system into dimensionless coordinates

a, u_2, H_2, ρ_2:

$$\bar{x} = \frac{x}{a},\ \bar{r} = \frac{r}{a},\ \bar{u} = \frac{u}{u_2},\ \bar{v} = \frac{v}{u_2},\ \bar{\varepsilon} = \frac{\varepsilon}{a u_2},$$

$$\bar{H} = \frac{H}{H_2},\ \bar{\rho} = \frac{\rho}{\rho_2},\ \bar{T} = \frac{T}{T_2},\ \bar{p} = \frac{p}{\rho_2 u_2^2},\ \bar{h}_2^* = \frac{h_2^*}{H_2}. \qquad (16)$$

For illustration, the governing equation for fuel conservation and transfer takes the following form:

$$\rho_2\bar{\rho}u_2\bar{u}\frac{\partial c_2}{a\partial\bar{x}} + \rho_2\bar{\rho}u_2\bar{v}\frac{\partial c_2}{a\partial\bar{r}} = \frac{1}{\mathrm{Sc}\,a\bar{r}}\frac{\partial}{a\partial\bar{r}}\left[\rho_2\bar{\rho}au_2\left(\frac{1}{\mathrm{Re}} + \bar{\nu}_t\right)a\bar{r}\frac{\partial c_2}{a\partial\bar{r}}\right] -$$

$$-7\cdot 10^8 \frac{c_1 c_2 \rho_2^2 \bar{\rho}^2}{m_1}\exp\left(-\frac{190300}{8,31441T}\right),$$

where the dimension ω_2 was transferred into the SI framework and incorporated $\rho_1 = c_1\rho$ и $\rho_2 = c_2\rho$.

By applying multiplication with $\frac{a}{\rho_2 u_2}$ to both sides, the following expression is derived:

$$\bar{\rho}\bar{u}\frac{\partial c_2}{\partial\bar{x}} + \bar{\rho}\bar{v}\frac{\partial c_2}{\partial\bar{r}} = \frac{1}{Sc\,\bar{r}}\frac{\partial}{\partial\bar{r}}\left[\bar{\rho}\left(\frac{1}{\mathrm{Re}} + \bar{\nu}_t\right)\bar{r}\frac{\partial c_2}{\partial\bar{r}}\right] + A_{r1}c_1c_2\bar{\rho}^2\exp\left(-\frac{A_{r2}}{T}\right).$$

$$\begin{cases} \bar{\rho}\bar{u}\dfrac{\partial\bar{u}}{\partial\bar{x}}+\bar{\rho}\bar{\vartheta}\dfrac{\partial\bar{u}}{\partial\bar{r}}=\dfrac{\partial}{\bar{r}\partial r}\left[\bar{\rho}\left(\dfrac{1}{\mathrm{Re}}+\bar{\nu}_t\right)\bar{r}\dfrac{\partial\bar{u}}{\partial\bar{r}}\right], \\ \dfrac{\partial\left(\bar{\rho}\bar{u}\bar{r}\right)}{\partial\bar{x}}+\dfrac{\partial\left(\bar{\rho}\bar{\vartheta}\bar{r}\right)}{\partial\bar{r}}=0, \\ \bar{\rho}\bar{u}\dfrac{\partial\bar{\bar{H}}}{\partial\bar{x}}+\bar{\rho}\bar{\vartheta}\dfrac{\partial\bar{\bar{H}}}{\partial\bar{r}}=\dfrac{1}{\mathrm{Pr}\,\bar{r}}\dfrac{\partial}{\partial\bar{r}}\left[\bar{\rho}\left(\dfrac{1}{\mathrm{Re}}+\bar{\nu}_t\right)\bar{r}\dfrac{\partial\bar{\bar{H}}}{\partial\bar{r}}\right], \\ \bar{\rho}\bar{u}\dfrac{\partial\bar{c}_2}{\partial\bar{x}}+\bar{\rho}\bar{\vartheta}\dfrac{\partial\bar{c}_2}{\partial\bar{r}}=\dfrac{1}{Sc\bar{r}}\dfrac{\partial}{\partial\bar{r}}\left[\bar{\rho}\left(\dfrac{1}{\mathrm{Re}}+\bar{\nu}_t\right)\bar{r}\dfrac{\partial\bar{c}_2}{\partial\bar{r}}\right]+A_{r1}c_1c_2\bar{\rho}^2\exp(-A_{r2}/T), \\ \bar{\rho}\bar{u}\dfrac{\partial\bar{\bar{C}}}{\partial\bar{x}}+\bar{\rho}\bar{\vartheta}\dfrac{\partial\bar{\bar{C}}}{\partial\bar{r}}=\dfrac{1}{Sc\bar{r}}\dfrac{\partial}{\partial\bar{r}}\left[\bar{\rho}\left(\dfrac{1}{\mathrm{Re}}+\bar{\nu}_t\right)\bar{r}\dfrac{\partial\bar{\bar{C}}}{\partial\bar{r}}\right], \\ \bar{\rho}\bar{u}\dfrac{\partial\bar{k}}{\partial\bar{x}}+\bar{\rho}\bar{\vartheta}\dfrac{\partial\bar{k}}{\partial\bar{r}}=\dfrac{1}{\delta_k\bar{r}}\dfrac{\partial}{\partial\bar{r}}\left(\bar{\rho}\bar{\nu}_t\bar{r}\dfrac{\partial\bar{k}}{\partial r}\right)+4\bar{\rho}\bar{\nu}_t\left(\dfrac{\partial\bar{u}}{\partial\bar{r}}\right)^2-\bar{\rho}\bar{\varepsilon}, \\ \bar{\rho}\bar{u}\dfrac{\partial\bar{\varepsilon}}{\partial\bar{x}}+\bar{\rho}\bar{\vartheta}\dfrac{\partial\bar{\varepsilon}}{\partial\bar{r}}=\dfrac{1}{\delta_\varepsilon\bar{r}}\dfrac{\partial}{\partial\bar{r}}\left(\bar{\rho}\bar{\nu}_t\bar{r}\dfrac{\partial\bar{\varepsilon}}{\partial\bar{r}}\right)+4c_1\left[1+\dfrac{A_1}{f_\mu}\right]^3\bar{\rho}\bar{\nu}_t\dfrac{\bar{\varepsilon}}{\bar{k}}\left(\dfrac{\partial\bar{u}}{\partial\bar{r}}\right)^2- \\ -c_2\left(1-e^{-\frac{\bar{k}^4}{\mathrm{Re}^2\bar{\varepsilon}^2}}\right)\bar{\rho}\dfrac{\bar{\varepsilon}^2}{\bar{k}}. \end{cases} \quad (17)$$

Here entered designation $f_\mu=\left(1-e^{-A_\mu\,\mathrm{Re}\sqrt{\bar{k}}r}\right)^2\left(1+A_t\dfrac{\bar{\varepsilon}}{\mathrm{Re}\,\bar{k}^2}\right)$.

$$T=\frac{H_1+\left(H_2-H_1\right)\bar{\bar{H}}-c_2h_2^*}{c_p},\quad \bar{\nu}_t=c_\mu f_\mu\frac{\bar{k}^2}{\bar{\varepsilon}}. \quad (18)$$

Considering straight-flow free expanded jets, and in accordance with established theoretical and experimental results, the static pressure may reasonably be regarded as constant: $p=const$ Bai Shi-I showed that in non-burning jets the static pressure variation is below 0.5% of the dynamic pressure, and Spaulding verified the same for burning jets through both theory and experiment. Consequently, the gas mixture equation of state is written as:

$$\bar{\rho}=\frac{m}{(m)_2\bar{T}}. \quad (19)$$

The second characteristic of the problem lies in the fact that the flow develops along the x-axis from left to right. Since the downstream region has no influence on the propagation processes, boundary conditions on the right-hand side are not specified. Consequently, the process can be adequately represented by parabolic equations. For this reason, Mises coordinates are employed, and the stream function is introduced according to the following relations:

$$\rho ur=\psi\frac{\partial\psi}{\partial r},\quad \rho vr=-\psi\frac{\partial\psi}{\partial x}. \quad (20)$$

The second relation in the system is satisfied in an unambiguous manner. To perform the calculation, the transverse coordinate is determined using the relation: $\frac{r^2}{2}=\int_0^\psi\frac{\psi d\psi}{\rho u}$.

Within the other equations of the system, the change of variables from coordinates (x, y) to coordinates (ξ, ψ) is performed using the relations:

$$\frac{\partial}{\partial x} = \frac{\partial}{\partial \xi} + \frac{\partial \psi}{\partial x}\frac{\partial}{\partial \psi} = \frac{\partial}{\partial \xi} - \frac{r}{\psi}\rho v \frac{\partial}{\partial \psi}, \qquad (21)$$
$$\frac{\partial}{\partial r} = \frac{\partial \psi}{\partial r}\frac{\partial}{\partial \psi} = \frac{r}{\psi}\rho u \frac{\partial}{\partial \psi}.$$

Accordingly, the right-hand parts of the equations take the following form:

$$\rho u \frac{\partial}{\partial x} + \rho v \frac{\partial}{\partial r} = \rho u \left[\frac{\partial}{\partial \xi} - \frac{r}{\psi}\rho v \frac{\partial}{\partial \psi}\right] + \rho v \frac{r}{\psi}\rho u \frac{\partial}{\partial \psi} = \rho u \frac{\partial}{\partial \xi}.$$

Thus, the left-hand sides of the equations become:

$$\frac{1}{r}\frac{\partial}{\partial r}\left(\rho \varepsilon r \frac{\partial}{\partial r}\right) = \frac{1}{r}\frac{r}{\psi}\rho u \frac{\partial}{\partial \psi}\left(\rho \varepsilon r \frac{r}{\psi}\rho u \frac{\partial}{\partial \psi}\right) =$$
$$= \frac{1}{\psi}\rho u \frac{\partial}{\partial \psi}\left(\frac{\rho^2 \varepsilon r^2 u}{\psi}\frac{\partial}{\partial \psi}\right).$$

$$\begin{cases} \dfrac{\partial u}{\partial \xi} = \dfrac{1}{\psi}\dfrac{\partial u}{\partial \psi}\left[\dfrac{\rho^2 u\, r^2 (\nu + \nu_t)}{\psi}\dfrac{\partial u}{\partial \psi}\right], \\ \dfrac{\partial H}{\partial \xi} = \dfrac{1}{\mathrm{Pr}\psi}\dfrac{\partial}{\partial \psi}\left[\dfrac{\rho^2 u\, r^2 (\nu + \nu_t)}{\psi}\dfrac{\partial u}{\partial \psi}\right], \\ \dfrac{\partial c_2}{\partial \xi} = \dfrac{1}{\mathrm{Sc}\psi}\dfrac{\partial}{\partial \psi}\left[\dfrac{\rho^2 u r^2 (\nu + \nu_t)}{\psi}\dfrac{\partial c_2}{\partial \psi}\right] + A_{r1}\dfrac{c_1 c_2 \rho^2}{u}\exp(-A_{r2}/T), \\ \dfrac{\partial \overline{\overline{C}}}{\partial \xi} = \dfrac{1}{\mathrm{Sc}\psi}\dfrac{\partial}{\partial \psi}\left[\dfrac{\rho^2 u r^2 (\nu + \nu_t)}{\psi}\dfrac{\partial \overline{\overline{C}}}{\partial \psi}\right], \\ \dfrac{\partial k}{\partial \xi} = \dfrac{1}{\psi}\dfrac{\partial}{\partial \psi}\left(\dfrac{r^2 u \rho^2}{\psi}\dfrac{\nu_t}{\delta_k}\dfrac{\partial k}{\partial \psi}\right) + 4\dfrac{\rho^2 r^2 u}{\psi^2}\nu_t\left(\dfrac{\partial u}{\partial \psi}\right)^2 - \dfrac{\varepsilon}{u}, \\ \dfrac{\partial \varepsilon}{\partial \xi} = \dfrac{1}{\delta_\varepsilon \psi}\dfrac{\partial}{\partial \psi}\left(\dfrac{\rho^2 u r^2}{\psi}\nu_t\dfrac{\partial \varepsilon}{\partial \psi}\right) + \\ + c_1\left[1 + \left(A_1 / f_\mu\right)^3\right]\dfrac{\varepsilon}{k}4\dfrac{\rho^2 u r^2}{\psi^2}\nu_t\left(\dfrac{\partial u}{\partial \psi}\right)^2 - c_2\left(1 - e^{-\frac{k^4}{\mathrm{Re}^2 \varepsilon^2}}\right)\dfrac{\varepsilon^2}{ku}, \end{cases} \qquad (22)$$

SOLUTION METHOD

Numerical way to solve the problem. Using basic radius a, flow rate u_2, density ρ_2, and enthalpy H_2, measurements were made in the system and conditions of equations, and Mises coordinates were entered (ξ,ψ). The mass displacement and retention equations for the components were reduced into one equation by introducing Schwab-Zeldovich functions and relative peak concentration $\tilde{\tilde{C}}$ [3,5]. As a result, the basic equations

$$\begin{cases} \dfrac{\partial u}{\partial \xi}=\dfrac{1}{\psi}\dfrac{\partial u}{\partial \psi}\left[\dfrac{\rho^2 u\ r^2(\nu+\nu_t)}{\psi}\dfrac{\partial u}{\partial \psi}\right], \\ \dfrac{\partial H}{\partial \xi}=\dfrac{1}{\Pr\psi}\dfrac{\partial}{\partial \psi}\left[\dfrac{\rho^2 u\ r^2(\nu+\nu_t)}{\psi}\dfrac{\partial u}{\partial \psi}\right], \\ \dfrac{\partial c_2}{\partial \xi}=\dfrac{1}{\mathrm{Sc}\psi}\dfrac{\partial}{\partial \psi}\left[\dfrac{\rho^2 u r^2(\nu+\nu_t)}{\psi}\dfrac{\partial c_2}{\partial \psi}\right]+A_{r1}\dfrac{c_1 c_2\,\bar{\rho}^2}{u}\exp(-A_{r2}/T), \\ \dfrac{\partial \tilde{\tilde{C}}}{\partial \xi}=\dfrac{1}{\mathrm{Sc}\psi}\dfrac{\partial}{\partial \psi}\left[\dfrac{\rho^2 u r^2(\nu+\nu_t)}{\psi}\dfrac{\partial \tilde{\tilde{C}}}{\partial \psi}\right], \\ \dfrac{\partial k}{\partial \xi}=\dfrac{1}{\psi}\dfrac{\partial}{\partial \psi}\left(\dfrac{r^2 u\rho^2}{\psi}\dfrac{\nu_t}{\delta_k}\dfrac{\partial k}{\partial \psi}\right)+4\dfrac{\rho^2 r^2 u}{\psi^2}\bar{\nu}_t\left(\dfrac{\partial u}{\partial \psi}\right)^2-\dfrac{\varepsilon}{u}, \\ \dfrac{\partial \varepsilon}{\partial \xi}=\dfrac{1}{\psi}\dfrac{\partial}{\partial \psi}\left(\dfrac{\rho^2 r^2 u}{\psi}\dfrac{\nu_t}{\delta_\varepsilon}\dfrac{\partial \varepsilon}{\partial \psi}\right)+4\dfrac{c_1\rho^2 r^2 u}{\psi^2}\bar{\nu}_t\dfrac{\varepsilon}{k}\times \\ \times\left[1+A_1\left(1-\mathrm{e}^{A_\mu \mathrm{Re}\sqrt{\bar{k}}r}\right)^{-2}\left(1+\dfrac{A_1\bar{\varepsilon}}{\mathrm{Re}\,\bar{k}^2}\right)^{-1}\right]^3\left(\dfrac{\partial u}{\partial \psi}\right)^2-c_2\left(1-e^{\frac{-\mathrm{Re}^2\varepsilon^2}{k^4}}\right)\dfrac{\varepsilon^2}{ku}, \end{cases} \quad (23)$$

$$T=\frac{H_1+(H_2-H_1)\bar{\bar{H}}-c_2 h_2^*}{c_p},$$

$$\bar{\rho}=\frac{mT_2}{(\mathrm{m})_2 T},\ \bar{\nu}_t=c_\mu f_\mu\frac{\bar{k}^2}{\bar{\varepsilon}}.$$

and the respective boundary conditions were set.

$0\le\bar{\psi}<1$: $\bar{u}=1,\bar{T}=1,\bar{\bar{C}}=1,\ c_n=(c_n)_2,k=k_2,\varepsilon=\varepsilon_2.\ 1\le\bar{\psi}<\bar{\psi}_\infty$:

$\bar{u}=\bar{u}_1,\bar{T}=\bar{T}_1,\bar{\bar{C}}=0,c_n=(c_n)_1,k=k_1,\varepsilon=\varepsilon_1.$

$$\xi>0\ ,\psi=0:\ \frac{\partial\bar{u}}{\partial\bar{\psi}}=0,\frac{\partial\bar{T}}{\partial\bar{\psi}}=0,\frac{\partial\bar{\bar{C}}}{\partial\psi}=0,\frac{\partial c_2}{\partial\psi}=0,\ \frac{\partial\bar{k}}{\partial\bar{\psi}}=0,\frac{\partial\varepsilon}{\partial\psi}=0. \quad (24)$$

$\psi\to\psi_\infty$: $\bar{u}=\bar{u}_1,\ \bar{T}=\bar{T}_1,c_2=(c_2)_1,\bar{\bar{C}}=0,\ k=k_1,\ \varepsilon=\varepsilon_1.$

The nonlinear equations in Mises coordinates were solved using a constant approximation method. [9-11].

$$\frac{\partial U}{\partial\bar{\xi}}=\frac{1}{\delta_U}\frac{\partial}{\bar{\psi}\partial\bar{\psi}}\left(K\lambda h_\psi\frac{\partial U}{\partial\bar{\psi}}\right)+f_U. \quad (25)$$

For the first group corresponding to $\lambda=\frac{1}{\mathrm{Re}}+\nu_t$, the following is introduced

$$\begin{aligned} U=u:&\ \delta_U=1,\ f_U=0; \\ U=\bar{\bar{H}}:&\ \delta_H=\mathrm{Pr},\ f_H=0; \\ U=\bar{\bar{C}}:&\ \delta_C=Sc,\ f_C=0; \\ U=c_2:&\ \delta_{c2}=Sc,\ f_{c2}=A_{r1}\frac{c_1c_2\bar{\rho}}{\bar{u}}\exp(-A_{r2}/T). \end{aligned} \quad (26)$$

In the preceding group, with $\lambda=\nu_t$ taken into account, the following two equations remain:

$$U = k:\ \delta_U = \delta_k,\ f_k = 4\frac{Kh_\psi}{\bar{\psi}}\lambda\left(\frac{\partial\bar{u}}{\partial\bar{\psi}}\right)^2 - \frac{\bar{\varepsilon}}{\bar{u}} = \bar{\mathrm{E}} - \frac{\bar{\varepsilon}}{\bar{u}},$$
$$U = \varepsilon:\ \delta_U = \delta_\varepsilon,\quad f_\varepsilon = \bar{E}\frac{\bar{\varepsilon}}{\bar{k}}\left[1+\left(\frac{A_1}{f_\mu}\right)^3\right] - c_2\left(1-e^{\frac{-k^4}{\varepsilon^2\,\mathrm{Re}^2}}\right)\frac{\bar{\varepsilon}^2}{\bar{k}}. \quad (27)$$

We now consider the approximation procedure for the equations. For the first group, the resulting expressions are as follows:

$$\lambda_j = \frac{1}{\mathrm{Re}} + \left(\bar{\nu}_t\right)_{i,j};$$

$$\frac{U^s_{i,j} - U_{i-1,j}}{h_\xi} = \frac{1}{2Sc_u\, jh^2_\psi}\times\left[\left(K_{i,j+1}\lambda_{j+1} + K_{i,j}\lambda_j\right)\left(U^s_{i,j+1} - U^s_{i,j}\right) - \right.$$
$$\left. -\left(K_{i,j}\lambda_j + K_{i,j-1}\lambda_{j-1}\right)\left(U^s_{i,j} - U^s_{i,j-1}\right)\right] + \left(f_u\right)^{s-1}_{i,j},$$

Multiply both sides of the equation by $2Sc_u h_\xi\, j$ also we will enter designation $\sigma = h_\xi / h^2_\psi$. Then we will receive

$$\sigma\left(K_{i,j+1}\lambda_{j+1} + K_{i,j}\lambda_j\right)U^s_{i,j+1} -$$
$$-\left[2Sc_u\, j + \sigma\left(K_{i,j+1}\lambda_{j+1} + K_{i,j}\lambda_j\right) + \sigma\left(K_{i,j}\lambda_j + K_{i,j-1}\lambda_{j-1}\right)\right]U^s_{i,j} +$$
$$+\sigma\left(K_{i,j}\lambda_j + K_{i,j-1}\lambda_{j-1}\right)U^s_{i,j-1} = -2Sc_u\, j\left(U_{i-1,j} + h_\xi\left(f_u\right)^{s-1}_{i,j}\right).$$

Let's designate

$$a^{(\mathrm{U})}_j = \sigma\left(K_{i,j+1}\lambda_{j+1} + K_{i,j}\lambda_j\right),\ c^{(\mathrm{U})}_j = \sigma\left(K_{i,j}\lambda_j + K_{i,j-1}\lambda_{j-1}\right),$$
$$b^{(\mathrm{U})}_j = 2Sc_U\, j + a^{(\mathrm{U})}_j + c^{(\mathrm{U})}_j,\ d^{(\mathrm{U})}_j = -2Sc_U\, j\left(U_{i-1,j} + h_\xi\left(f_U\right)^{s-1}_{i,j}\right).$$

Then the finite difference equation takes the form:

$$a^{(\mathrm{U})}_j U^s_{i,j+1} - b^{(\mathrm{U})}_j U^s_{i,j} + c^{(\mathrm{U})}_j U^s_{i,j-1} = d^{(\mathrm{U})}_j. \quad (28)$$

If we believe that

$$U^s_{i,j-1} = \alpha^{(\mathrm{U})}_{j-1} U^s_{i,j} + \beta^{(\mathrm{U})}_{j-1},$$

Consequently, the fit coefficients corresponding to the internal nodes are determined as follows:

$$\alpha^{(\mathrm{U})}_j = \frac{a^{(\mathrm{U})}_j}{b^{(\mathrm{U})}_j - \alpha^{(\mathrm{U})}_{j-1}c^{(\mathrm{U})}_j},\ \beta^{(\mathrm{U})}_j = \frac{-d^{(\mathrm{U})}_j + c^{(\mathrm{U})}_j\beta^{(\mathrm{U})}_{j-1}}{b^{(\mathrm{U})}_j - \alpha^{(\mathrm{U})}_{j-1}c^{(\mathrm{U})}_j} \quad (29)$$

The first $S_{\min}$ approach is performed without check of approach condition and replacement

$$\tilde{u}^{s-1}_{i,j} = \tilde{u}^s_{i,j},\quad \tilde{H}^{s-1}_{i,j} = \tilde{H}^s_{i,j},$$
$$\tilde{\rho}^{s-1}_{i,j} = \tilde{\rho}^s_{i,j},\quad \tilde{C}^{s-1}_{i,j} = \tilde{C}^s_{i,j} \quad . \quad (30)$$

Later $S_{\min}$ - the convergence condition is checked $\max_{j\in[0;\,N_j]}\left|\tilde{H}^{s-1}_{i,j} - \tilde{H}^s_{i,j}\right| < \varepsilon_t$.

If convergence conditions are reached, the system moves to the next layer at. Otherwise, the s-th approach is accepted

$$\tilde{u}_{i,j}^{s-1} = \tilde{u}_{i,j}^{s}, \quad \tilde{H}_{i,j}^{s-1} = \tilde{H}_{i,j}^{s},$$

$$\rho_{i,j}^{s-1} = \rho_{i,j}^{s}, \quad \tilde{C}_{i,j}^{s-1} = \tilde{C}_{i,j}^{s}$$

and proceeds to the next approximation.

Once the convergence criteria for the newly computed parameter values are fully satisfied, additional quantities of interest—such as the integrals of excess momentum, total enthalpy, and the residual (unburned) fuel fraction in the corresponding cross-section—can be evaluated if necessary.

In the numerical domain, the upper bound of the dimensionless radial coordinate was set to 20, and new discrete step sizes were introduced along both the longitudinal and radial directions. The calculation along the longitudinal axis proceeded until the value of the conservative scalar function at the centerline decreased below 0.05, indicating near-complete combustion.

The results were saved in three files. The first file comprised the axial velocity, enthalpy, turbulence factor of the cross-section, radial flame coordinates via linear interpolation, boundary layer speed $b(x)$, and observational measurements.

The second file contains information on radial coordinate variations of velocity, enthalpy, temperature, concentration, and turbulence at selected points. A dedicated algorithm was applied to convert the regular flow line steps into dimensionless radial coordinates, using linear interpolation as implemented in algorithm h_y for plotting.

The third output file contained the data necessary for constructing isothermal contours within the temperature field. These data were stored in physical (non-transformed) coordinates to facilitate post-processing. Due to certain limitations—particularly constraints in the computational domain and the lack of advanced visualization tools in the Pascal ABS environment—the graphical representation of the results could not be performed within the simulation code. Therefore, all isothermal plots and visualizations were generated using Microsoft Excel.

RESULTS

In this study, the analysis is focused specifically on examining how the temperature of individual gas components influences the isothermal contours and species concentration profiles.

The combustible reaction includes methane gas and nitrogen. $(c_1)_1 = 0.232,\ (c_5)_1 = 0.768, (c_2)_2 = 1$. The velocity of the main stream - 61 m/s, velocity of satellite current – 18.3 m/s. $T_1 = 1000\ K$ whence $T_2 = 293K$ and $T_2 = 400K$ because they are $\bar{x} = 40$ and $\bar{x} = 100$ the diagrams show the concentration of.

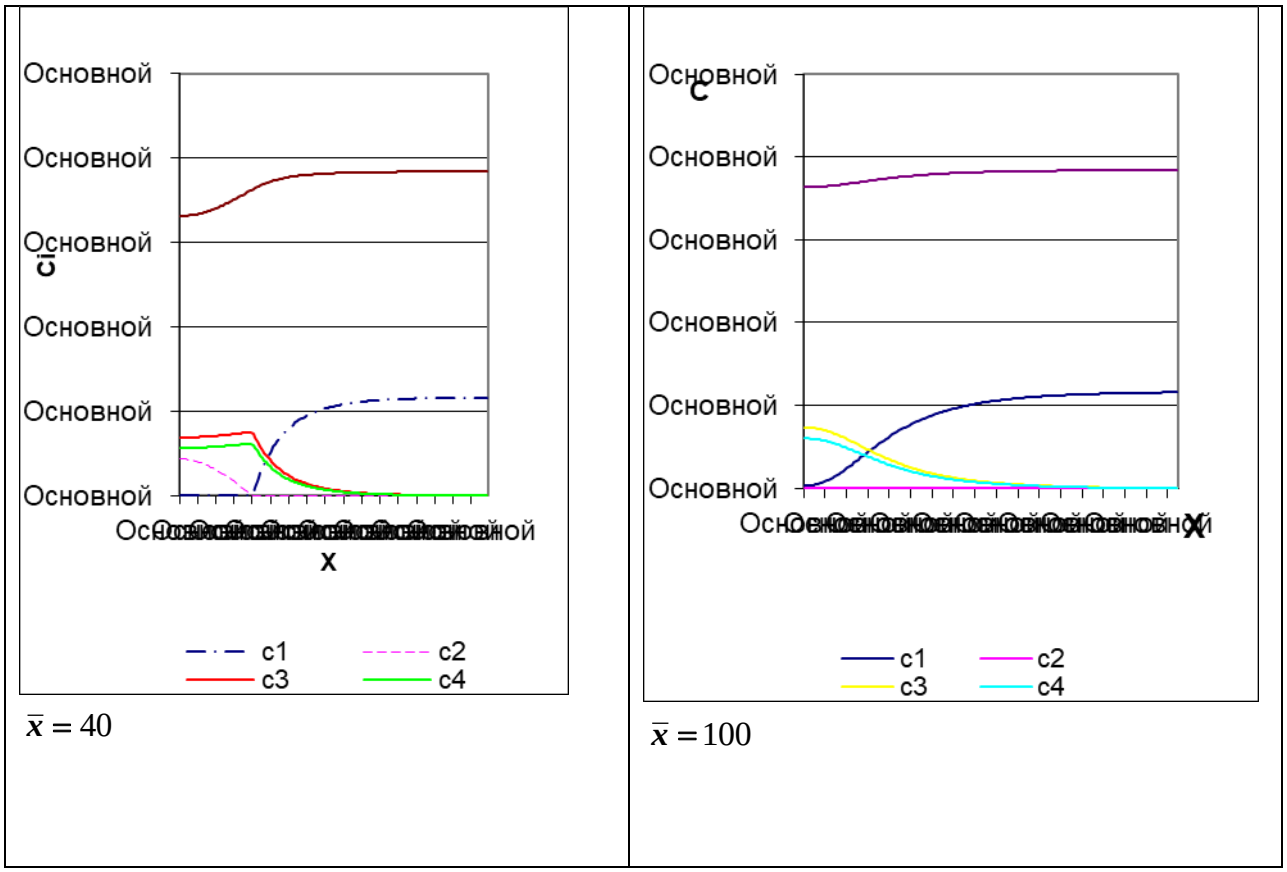

$\bar{x} = 40$ $\bar{x} = 100$

Fig. 2. $T_1 = 1000\,K$ and $T_2 = 293\,K$ of concentrations.

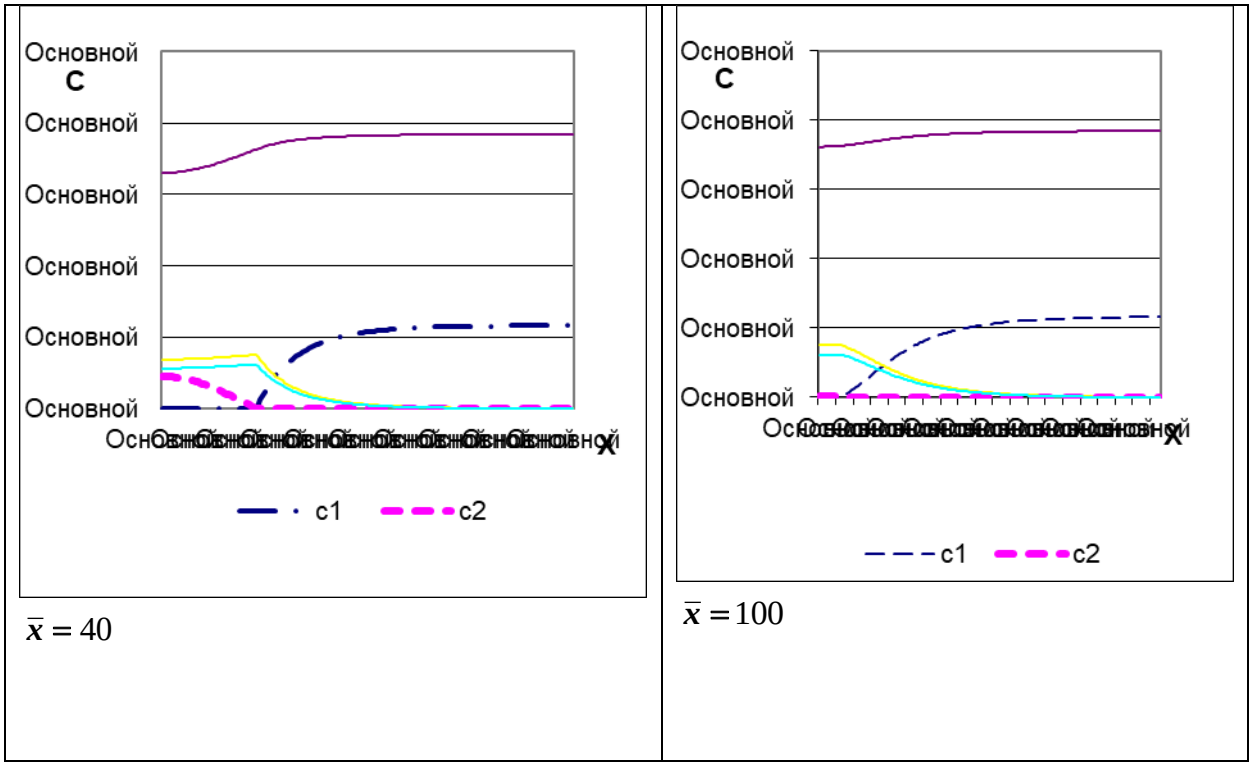

$\bar{x} = 40$ $\bar{x} = 100$

Fig. 3. $T_1 = 1000\,K$ and $T_2 = 400\,K$ of concentrations.

As illustrated in the graph, the fuel core experiences disruption at the boundary layer speed $\bar{x} = 40$.

Concentration view after the flame $T_1 = 1000\,K$ and $T_2 = 293\,K$, $\bar{x} = 100$ as shown in the diagram above. $T_1 = 1000\,K$ and $T_2 = 400\,K$ when $\bar{x} = 100$ in the cross-section. Based on the obtained results, it can be concluded that higher initial temperatures lead to prolonged combustion and extended flame development. Similar trends were observed in the distributions of velocity, total enthalpy, and turbulence intensity, although their spatial extents remained significantly shorter compared to the initial flame length.

Analysis under identical initial conditions shows that the methane flame is shorter and broader than the propane flame, due to the reduced momentum flux of the methane jet.

$T_1 = 1000\ K$ when $T_2 = 293\ K$ and $T_2 = 400K$ here is an example of the isotherms that are

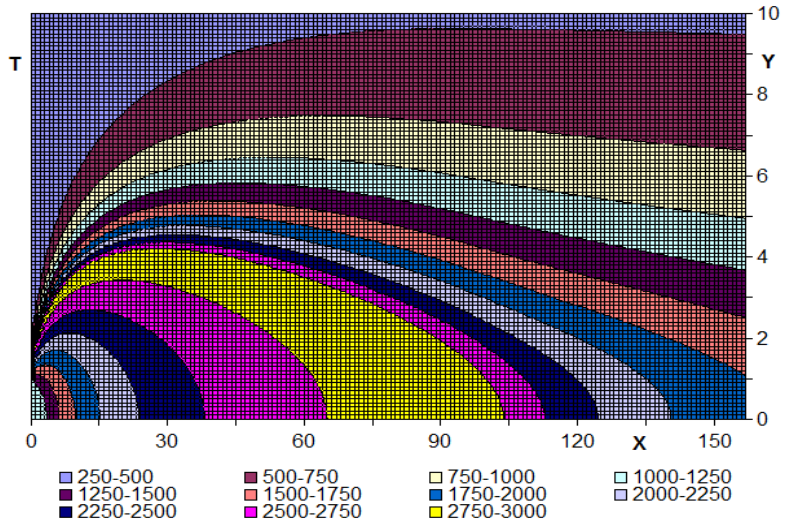

Fig. 4. $T_1 = 1000\ K$ and $T_2 = 293\ K$

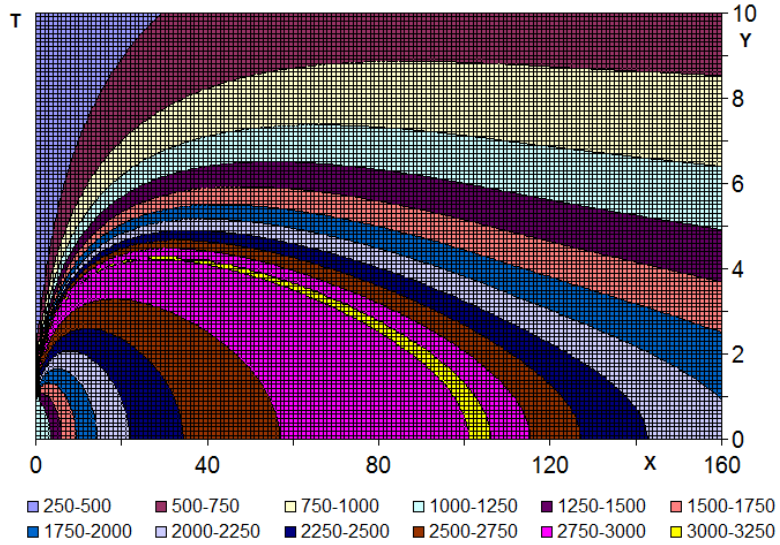

Fig. 5. $T_1 = 1000\ K$ and $T_2 = 400K$

Maximum temperature in the first case T=2929K and in the latter case $T^* = 3018.84$ values were calculated.

FINDINGS

As the temperature field develops, the maximum temperature is observed along the axis of symmetry near the flame tip. Numerical results indicate that increasing the initial fuel temperature leads to a reduction in flame length, while higher air temperatures result in longer flames. The former effect is attributed to reduced fuel consumption, whereas the latter is associated with the increased oxygen availability in preheated air. Overall, the findings demonstrate that the thermal characteristics and flame structure of methane combustion in an airstream differ significantly from those of propane, particularly in terms of flame shape and temperature distribution.

References

1. J. H. Park, Three-Dimensional Nonequilibrium Numerical Modeling of Arc-Anode Attachment in Direct-Current Electric Arcs, Ph.D. Thesis, University of Minnesota, 2003.
2. Gordon, S. and B. J. McBride (1994). Computer program for calculation of complex chemical equilibrium compositions and applications Part I: Analysis. Reference Publication NASA-RP-1311, NASA Glenn Research Center.
3. International Energy Agency (2009). CO2 emissions from fuel combustion 2009 edition.Technical report, International Energy Agency.
4. S. B. Pope, Ten questions Concerning the Large-Eddy Simulation of Turbulent Flows, New Journal of Physics, 2004, 6(35)
5. A. A. Iordanidis and C. M. Franck, Self-consistent Radiation-based Simulation of Electric Arcs: II. Application to Gas Circuit Breakers, J. Phys. D: Appl. Phys., 2008, 41, 135206, p 1-9.
6. Абрамович Г.Н. Теория турбулентных струй. М.: «Наука». 1984. 715 с.
7. Кузнецов В.Р., Сабельников В.А. Турбулентность и горение. М.: «Наука» 1986. 288 с.
8. Баев В.К., Головичев В.К., Третьяков П.К. Горение в сверхзвуковом потоке. Новосибирск. Наука. 1984. 304 с.
9. Алиев Ф., Жумаев З.Ш. Струйные течения реагирующих газов.Ташкент, Фан, 1987.132 с.
10. Edelman R.B. and Harsha P.T. Some observations on turbulent mixing with chemical reactions//AIAA. Aerospace Science Meeting, 15-th, New-York, 1977, Technical Paper, pp. 55-102.
11. "Numerical Grid Generation," ed. J. F. Thompson, Elsevier Sci. Pub., (1982).
12. Launder, B. E. and D. B. Spalding, "The Numerical Calculation fo Turbulent Flows, Computational Methods Applied to Mechanics and Engineering, Vol. 3,269-289, (1974).

13. Gordon, S. and B. J. McBride, "Computer Program for Calculation of Complex Chemical Equilibrium Compositions, Rocket Performance, Incident and Reflected Shocks, and Chapman-Jonquet Detonations," NASA SP-273, (1976), new version (1989).
14. Lallemant, N., R. Dugue, and R. Weber (2003). Measurements techniques for studying oxy-natural gas ames. Journal of the Institute of Energy 76.
15. Yin, C., L. C. R. Johansen, L. Rosendahl, and S. Kr (2010). Models for gas radiation properties applicable to CFD modeling of oxy-fuel combustion. Paper submitted to the 33r

Author contributions

•**Khujayev I.K.** – Conceptualization, Methodology, Supervision, Writing – Review and Editing.

•**Ergashev D.Y.** – Data Curation, Formal Analysis, Visualization, Writing – Original Draft Preparation.

Acknowledgements

The authors would like to express their sincere gratitude to for valuable guidance and insightful discussions throughout this research. Special thanks are also extended to the [Institute of Mechanics and Seismic Stability of Structures named after M.T.Urazbaev, Uzbekistan Academy of Sciences] for providing the necessary facilities and computational resources.

Biographies



Khujaev Ismatulla received his Doctor of Science (DSc) degree in mechanics from the Institute of Mechanics and Seismic Stability of Structures named after M.T. Urazbaev, Academy of Sciences of Uzbekistan, Tashkent. He is currently working at the same institute. His current research interests include fluid and gas dynamics.



Ergashev Dilshodjon Ergashev Dilshodjon holds a Master's degree in Ground Vehicles and Systems. He is currently a PhD student at the Urazbayev Institute of Mechanics and Seismic Stability of Structures. His current research interests include fluid and gas mechanics.